Chase, B.M., et al., 2019, Orbital controls on Namib Desert hydroclimate over the past 50,000 years: Geology, https://doi.org/10.1130/G46334.1

Supplementary Material

Methods

The rock hyrax middens were collected and processed following Chase et al. (2012). Radiocarbon age determinations (n=86) were processed at the ^{14}CHRONO Centre, Queen's University Belfast using accelerator mass spectrometry (AMS) (Table S1; Fig. S1). Samples were pre-treated with 2% HCl for one hour at room temperature to remove carbonates and dried at 60°C. They were then weighed into quartz tubes with an excess of CuO, sealed under vacuum and combusted to CO_2. The CO_2 was converted to graphite on an iron catalyst using the zinc reduction method (Slota et al., 1987). The radiocarbon ages were corrected for isotope fractionation using the AMS measured $\delta^{13}C$ and calibrated using the SHCal13 calibration data (Hogg et al., 2013). The Bayesian Bacon 3.0.3 software package (Blaauw and Christen, 2011) was used to generate all age-depth models (Fig. S1).

The stable nitrogen isotope composition of 1792 overlapping hyraceum samples (approx. 3 mg) were measured at the School of Geography, Geology and the Environment, University of Leicester, with contiguous/overlapping samples obtained from two offset tracks using a 1 mm drill. Isotope ratios were measured on a Sercon 20-20 isotope ratio mass spectrometer. Samples were combusted at 1020ºC and the nitrogen converted into N_2 in a Sercon ANCA GSL elemental analyser interfaced to the mass spectrometer. The standard deviation derived from replicate analyses of homogeneous material was better than 0.2‰. Results are expressed relative to atmospheric nitrogen (Fig. S1).

Plant wax *n*-alkanes were extracted from 100-200 mg of hyraceum using an accelerated solvent extractor (ASE-200, Dionex) following a procedure described by Niedermeyer (Niedermeyer et al., 2016). The δD values of individual *n*-alkanes in toluene were measured using a Thermo Trace 1310 coupled to a ThermoFinnigan DELTA V plus isotope-ratio mass spectrometer via a pyrolysis furnace operated at 1420°C. The GC oven was

equipped with a Thermo TG 5 MS column (30 m × 0.25 mm × 1 μm). The GC oven was programmed at 120°C for 2 min, ramped at 4°C min^{-1} to 310°C, rand held for 15 min. Data processing and H_{3+} correction used the Isodat software as described by Sessions et al. (Sessions et al., 2001) using a H_2 reference gas with known hydrogen isotopic composition. The δD record of the *n*-C_{31} alkane (which was the most abundant homologue throughout the record) was corrected for glacial−interglacial changes of ice volume using the $\delta^{18}O_{seawater}$ reconstruction of Shackleton et al. (Shackleton, 2000). Using the modern Global Meteoric Waterline, changes of $\delta^{18}O_{seawater}$ were multiplied by 8 to approximate corresponding changes of $\delta D_{seawater}$ values, which were in turn subtracted from the *n*-C_{31} δD record (Schefuß et al., 2005).

To create our composite $\delta^{15}N$ record from the 1792 samples from the eight rock hyrax middens considered in this study together, we combined and smoothed the age-ranked ensemble using Gaussian kernel-based interpolation (Fig. S2). This technique has been shown to be the most appropriate to interpolate irregularly sampled time series, such as those obtained from the Namib middens (Fig. S1). We followed the recommendation of Rehfeld et al. (Rehfeld et al., 2011) and used the average temporal resolution of the record (28.08 years) to define the width of our Gaussian kernel. To maintain the true temporal resolution of our composite record, the values were interpolated at the sample ages.

The composite record for wind strength in the Southeast Atlantic (Figure 2d) was calculated according to the same method using the data of Farmer et al., (Farmer et al., 2005), Little et al., (Little et al., 1997), Stuut et al., (Stuut et al., 2002) and Pichevin et al., (Pichevin et al., 2005).

For the modelling component of this study we employed climate data from the TraCE21ka experiment (He et al., 2013; Liu et al., 2009; Otto-Bliesner et al., 2014). TraCE21ka used the Community Climate System Model ver. 3; (CCSM3; Collins et al., 2006)

a global coupled atmosphere – ocean – sea ice – land general circulation model that has a latitude – longitude resolution of ~3.75° in the atmosphere and ~3° in the ocean and includes a dynamic global vegetation module. The simulation includes transient orbitally forced insolation changes and changes in the atmospheric concentrations of carbon dioxide, methane and nitrous oxide, as well as the evolution of ice sheets and their meltwater contributions to the ocean. The climate data have been regridded using bilinear interpolation to a spatial resolution of 2.5 x 2.5° (latitude/longitude) (Fordham et al., 2017).

Interpretation of stable isotope proxies

Hyraceum $\delta^{15}N$ has been shown - through observation of modern middens and plants (Carr et al., 2016; Murphy and Bowman, 2006), as well as comparison with independent records and other proxies obtained from the same midden samples, to reflect environmental water availability, with higher $\delta^{15}N$ values occurring during more arid periods (Chase et al., 2015a; Chase et al., 2015b; Chase et al., 2009). This relationship between $\delta^{15}N$ and water availability is considered to reflect the more "open" nitrogen cycle in arid regions (Amundson et al., 2003; Austin and Vitousek, 1998; Handley et al., 1999). Fractionating pathways in the soil (nitrification, denitrification, etc.) mean that nitrogen lost through transformation and the release of gaseous products is depleted in ^{15}N, and the nitrogen remaining (which represents a rather small pool in arid regions) is enriched. While in more humid regions N is cycled between live and dead organic pools, in drier regions more N flows to mineral pools where it is subject to gaseous loss (McCalley and Sparks, 2009), and the $\delta^{15}N$ value of soils is thus higher under conditions of increased aridity (Amundson et al., 2003; Austin and Vitousek, 1998; Handley et al., 1999). This variation in soil ^{15}N has been shown to be transferred through the food chain from plants to hyrax body tissue and ultimately, to hyraceum (Carr et al., 2016).

While hyraceum $\delta^{15}N$ most closely reflects aridity (defined here specifically as precipitation *minus* potential evapotranspiration), at low latitudes δD values of precipitation are predominantly controlled by continentality and amount effects (Dansgaard, 1964), with increased distance from source and/or precipitation amount/intensity resulting in lower values (Bowen, 2008; Dansgaard, 1964; Niedermeyer et al., 2016). Studies of leaf wax δD indicate strong linear relationships with precipitation δD (Garcin et al., 2012; Hou et al., 2008), although evapotranspiration and vegetation type may also exert relatively limited secondary influences (Collins et al., 2014; Garcin et al., 2012; Herrmann et al., 2017; Sachse et al., 2012). As such, the δD and $\delta^{15}N$ records from the Namibian middens each provide independent insights into distinct aspects of regional hydroclimates, with δD primarily reflecting changes in rainfall source and amount/intensity and $\delta^{15}N$ reflecting changes in moisture balance, including the influence of temperature change on evapotranspiration and general water availability. Trends in the two records must therefore be compared with care. However, these interpretations are consistent with the broad similarities between the Spitzkoppe δD and $\delta^{15}N$ records, but also highlight the role of lower glacial-age temperatures on aridity. For example, less rainfall is necessary to create conditions of equivalent humidity during the cooler glacial period. Thus higher leaf wax δD (less rainfall) corresponds with lower hyraceum $\delta^{15}N$ (more humid) during the last glacial period compared with the Holocene, as precipitation is more effective under lower temperatures.

Table S1: Radiocarbon ages and calibration information for the rock hyrax middens considered in this study.

Sample	^{14}C age yr BP	1 sigma error	calibration data	95.4 % (2σ) cal age ranges lower cal range BP	upper cal range BP	relative area under distribution	median probability (cal BP)
PEL-1-1							
UBA-22377	1302	26	SHCal13	1091	1153	0.247237	1209
				1156	1270	0.752763	

UBA-22378	3950	29	SHCal13	4185	4186	0.000744	4342
				4194	4195	0.000651	
				4235	4435	0.998605	
UBA-22379	5767	33	SHCal13	6414	6426	0.021415	6519
				6434	6635	0.978585	
UBA-22380	8720	39	SHCal13	9538	9747	0.994915	9624
				9753	9761	0.005085	
UBA-22381	18408	94	SHCal13	21942	22446	1	22238
UBA-22382	23725	163	SHCal13	27501	28086	1	27778
UBA-22383	25785	194	SHCal13	29409	30539	1	29947
UBA-22384	27717	239	SHCal13	31062	32043	1	31450
UBA-22385	34526	533	SHCal13	37632	40279	1	39007
UBA-22386	41451	785	SHCal13	43380	46159	1	44832
PEL-1-2							
UBA-21242	783	22	SHCal13	657	694	0.772203	677
				696	722	0.227797	
UBA-22389	1648	26	SHCal13	1420	1545	0.973696	1495
				1550	1560	0.026304	
UBA-22390	2492	30	SHCal13	2359	2548	0.566942	2359
				2554	2620	0.17186	
				2628	2705	0.261198	
UBA-22391	4588	30	SHCal13	5049	5194	0.618628	5049
				5212	5317	0.381372	
UBA-22392	8461	39	SHCal13	9308	9361	0.114364	9308
				9376	9381	0.007013	
				9396	9527	0.878622	
UBA-22393	13841	60	SHCal13	16402	16949	1	16676
UBA-22394	19415	103	SHCal13	23000	23628	1	23323
UBA-22395	21215	150	SHCal13	25175	25822	1	25513
UBA-22396	22399	137	SHCal13	26217	27081	1	26638
UBA-21243	24426	126	SHCal13	28080	28731	1	28429
PEL-1-4a							
UBA-21248	59	27	SHCal13; SHZ1_2	-6	-5	0.151	
				31	56	0.554	
				122	132	0.295	
UBA-22397	314	23	SHCal13	292	331	0.47284	370
				365	443	0.52716	
UBA-22398	716	23	SHCal13	564	600	0.477449	632
				630	668	0.522551	

UBA-22399	998	25	SHCal13	800	922	1	856
UBA-22400	1084	24	SHCal13	918	979	0.99881	946
				1039	1040	0.00119	
UBA-21249	1320	27	SHCal13	1095	1144	0.093643	1223
				1171	1278	0.906357	
SPZ2012-1-1							
UBA-21254	111	19	SHCal13; SHZ1_2	-6	-5	0.005	
				-4	-4	0	
				3	14	0.029	
				16	72	0.514	
				83	106	0.087	
				112	141	0.27	
				227	250	0.095	
UBA-25236			SHCal13	506	548	1	528
UBA-23991			SHCal13	1535	1619	0.779236	1588
				1653	1698	0.220764	
UBA-25237			SHCal13	1611	1758	0.7415	1722
				1761	1823	0.2585	
UBA-23981			SHCal13	2153	2316	1	2231
UBA-25238			SHCal13	2349	2517	0.772982	2447
				2526	2538	0.011494	
				2588	2616	0.052277	
				2633	2698	0.163247	
UBA-23982			SHCal13	2744	2866	1	2794
UBA-23983			SHCal13	2622	2627	0.00419	2745
				2707	2778	0.99581	
UBA-25239			SHCal13	2965	3174	1	3082
UBA-23984			SHCal13	3397	3561	1	3471
UBA-25240			SHCal13	3900	4104	0.895792	4029
				4106	4149	0.104208	
UBA-23985			SHCal13	4418	4616	0.964502	4502
				4765	4784	0.035498	
UBA-25241			SHCal13	4424	4629	0.905155	4538
				4637	4642	0.004565	
				4683	4687	0.004439	
				4762	4798	0.085841	
UBA-23986			SHCal13	5046	5205	0.638623	5162
				5210	5312	0.361377	
UBA-25242			SHCal13	5302	5339	0.206586	5405
				5341	5467	0.793414	
UBA-23987			SHCal13	5667	5671	0.005721	5817

				5714	5909	0.994279	
UBA-25243			SHCal13	5992	6211	0.980332	6102
				6248	6264	0.019668	
UBA-23988			SHCal13	6307	6472	1	6388
UBA-25244			SHCal13	6669	6859	0.985138	6762
				6871	6879	0.014862	
UBA-23989			SHCal13	7168	7317	1	7251
UBA-25245			SHCal13	7674	7852	0.994071	7760
				7908	7913	0.005929	
UBA-23990			SHCal13	8048	8099	0.092523	8214
				8101	8121	0.026364	
				8131	8141	0.013611	
				8151	8332	0.867502	
UBA-25246			SHCal13	8720	9020	1	8884
UBA-21255			SHCal13	8781	8832	0.047674	9028
				8862	8919	0.041032	
				8954	8962	0.003044	
				8968	9137	0.883718	
				9176	9203	0.013824	
				9220	9241	0.010708	
SPZ2012-1-2_3rd							
UBA-28912	9507	37	SHCal13	10575	10794	0.894994	10705
				10855	10859	0.002874	
				10962	11007	0.047634	
				11020	11065	0.054499	
UBA-28913	12267	45	SHCal13	13959	14310	1	14120
UBA-28914	13554	61	SHCal13	16049	16523	1	16268
UBA-28915	13644	50	SHCal13	16190	16628	1	16388
SPZ2012-1-2							
UBA-21256	448	22	SHCal13	339	353	0.060692	485
				450	508	0.939308	
UBA-25247	1460	24	SHCal13	1290	1358	1	1315
UBA-24096	2700	28	SHCal13	2742	2844	1	2771
UBA-25248	3429	37	SHCal13	3483	3489	0.003871	3631
				3491	3534	0.0453	
				3549	3724	0.925912	
				3755	3756	0.000698	
				3795	3818	0.024217	
UBA-24097	5277	26	SHCal13	5915	6027	0.798667	5978
				6046	6066	0.027512	

				6077	6117	0.114318	
				6151	6176	0.059503	
UBA-25249	6091	37	SHCal13	6757	6762	0.004029	6899
				6780	7006	0.990056	
				7133	7140	0.005916	
UBA-24098	7517	31	SHCal13	8199	8373	1	8297
UBA-25250	9308	42	SHCal13	10281	10571	1	10444
UBA-24099	12727	48	SHCal13	14839	15288	1	15107
UBA-24100	13519	66	SHCal13	15989	16487	1	16219
UBA-21257	13886	57	SHCal13	16491	17007	1	16758
UBA-24101	13992	54	SHCal13	16636	17149	1	16922
UBA-24102	14309	52	SHCal13	17155	17570	1	17379
UBA-24103	14657	50	SHCal13	17615	17975	1	17797
UBA-24104	15088	63	SHCal13	18050	18485	1	18282
UBA-24105	16731	64	SHCal13	19919	20364	1	20134
UBA-21258	17918	72	SHCal13	21409	21886	1	21663
SPZ2013-1							
UBA-25785	17866	84	SHCal13	21311	21864	1	21594
UBA-28916	20805	97	SHCal13	24593	25347	1	25042
UBA-25786	21102	119	SHCal13	25110	25692	1	25411
UBA-25787	21618	126	SHCal13	25630	26076	1	25860
UBA-28917	22426	130	SHCal13	26261	27100	1	26678
UBA-28918	23073	128	SHCal13	27089	27592	1	27353
UBA-25788	24344	170	SHCal13	27928	28707	1	28333
UBA-28919	24693	175	SHCal13	28267	29096	1	28687
UBA-28920	25133	157	SHCal13	28751	29520	1	29129
UBA-28921	25542	161	SHCal13	29152	30195	1	29610
UBA-25789	26024	211	SHCal13	29625	30759	1	30231
UBA-25790	26365	222	SHCal13	29982	31005	1	30602
UBA-25791	27883	321	SHCal13	31119	32589	1	31681
ZIZ-1-1							
UBA-24433	3099	21	SHCal13	3179	3203	0.066032	3271
				3205	3356	0.933968	
UBA-9007	3029	22	SHCal13	3062	3250	0.973996	3163
				3302	3324	0.026004	
UBA-9008	14335	47	SHCal13	17197	17597	1	17415
UBA-24434	14626	50	SHCal13	17584	17949	1	17766
UBA-24435	16081	53	SHCal13	19168	19557	1	19362

UBA-9009	16781	52	SHCal13	19992	20401	1	20190
UBA-24436	17059	58	SHCal13	20305	20721	1	20526
UBA-9010	18114	57	SHCal13	21662	22140	1	21894
UBA-24437	18670	82	SHCal13	22323	22712	1	22488
UBA-24438	20942	104	SHCal13	24883	25566	1	25234
UBA-24439	23594	135	SHCal13	27460	27900	1	27687
UBA-24440	29929	287	SHCal13	33532	34532	1	33991
UBA-9432	32287	155	SHCal13	35735	36477	1	36139
UBA-24441	33763	447	SHCal13	36669	39074	1	38030
ZIZ-1-3b							
Pta-9680	15030	341	SHCal13	17407	18930	1	18204
UBA-24442	17985	78	SHCal13	21469	21965	1	21737
UBA-9433	19230	70	SHCal13	22875	23417	1	23117
UBA-24444	22034	118	SHCal13	25944	26518	1	26198
UBA-24445	24777	155	SHCal13	28405	29156	1	28769
UBA-24446	29339	263	SHCal13	32863	33969	1	33488
UBA-24447	30173	259	SHCal13	33758	34649	1	34181
UBA-24448	32063	386	SHCal13	35010	36744	1	35904
UBA-9211	32358	159	SHCal13	35792	36571	1	36206
UBA-24449	33703	570	SHCal13	36397	39258	1	37918
Pta-9686	34250	1600	SHCal13	35137	41669	1	38489

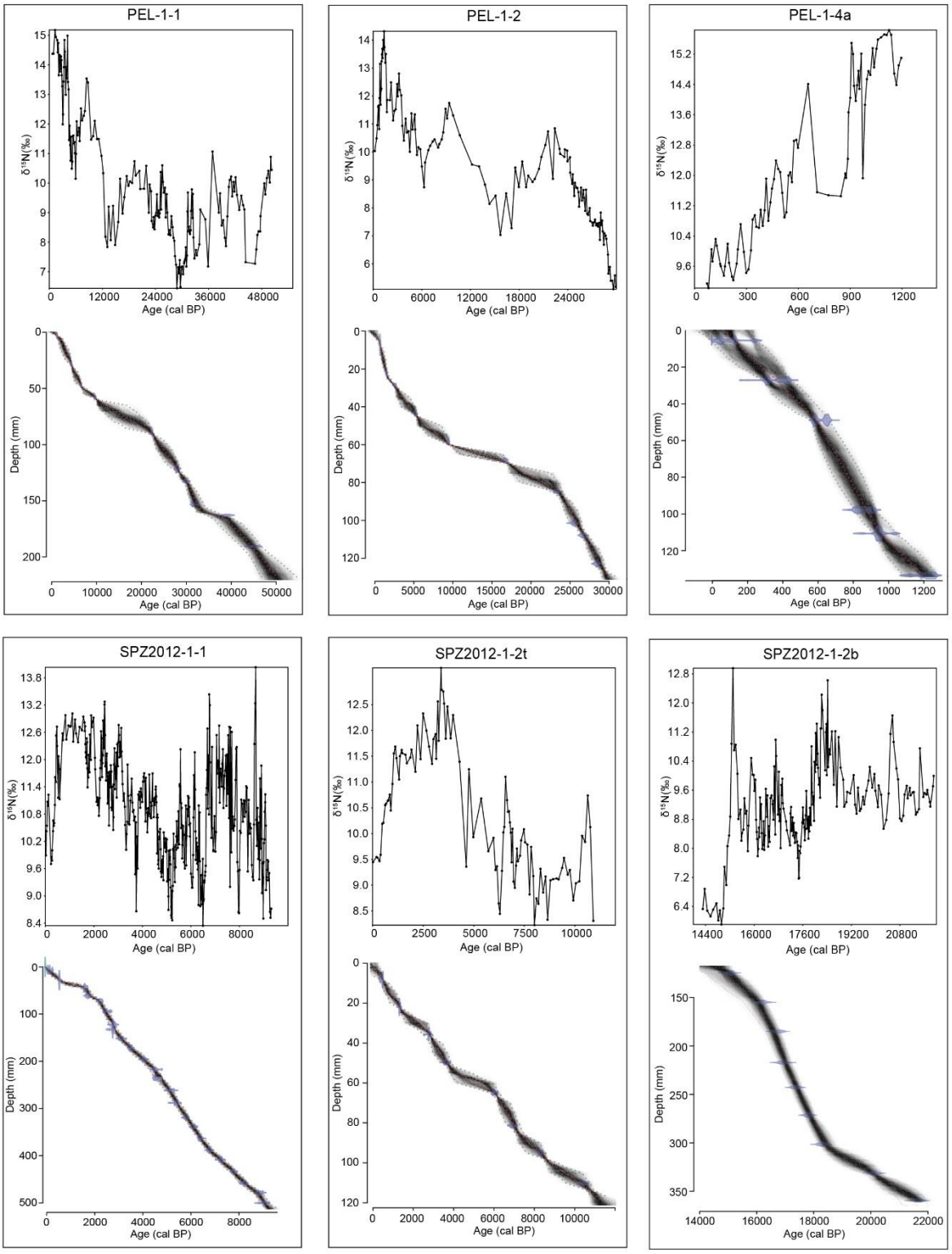
PEL-1-1
δ15N(‰)
Age (cal BP)
Depth (mm)
PEL-1-2
δ15N(‰)
Age (cal BP)
Depth (mm)
PEL-1-4a
δ15N(‰)
Age (cal BP)
Depth (mm)
SPZ2012-1-1
δ15N(‰)
Age (cal BP)
Depth (mm)
SPZ2012-1-2t
δ15N(‰)
Age (cal BP)
Depth (mm)
SPZ2012-1-2b
δ15N(‰)
Age (cal BP)
Depth (mm)

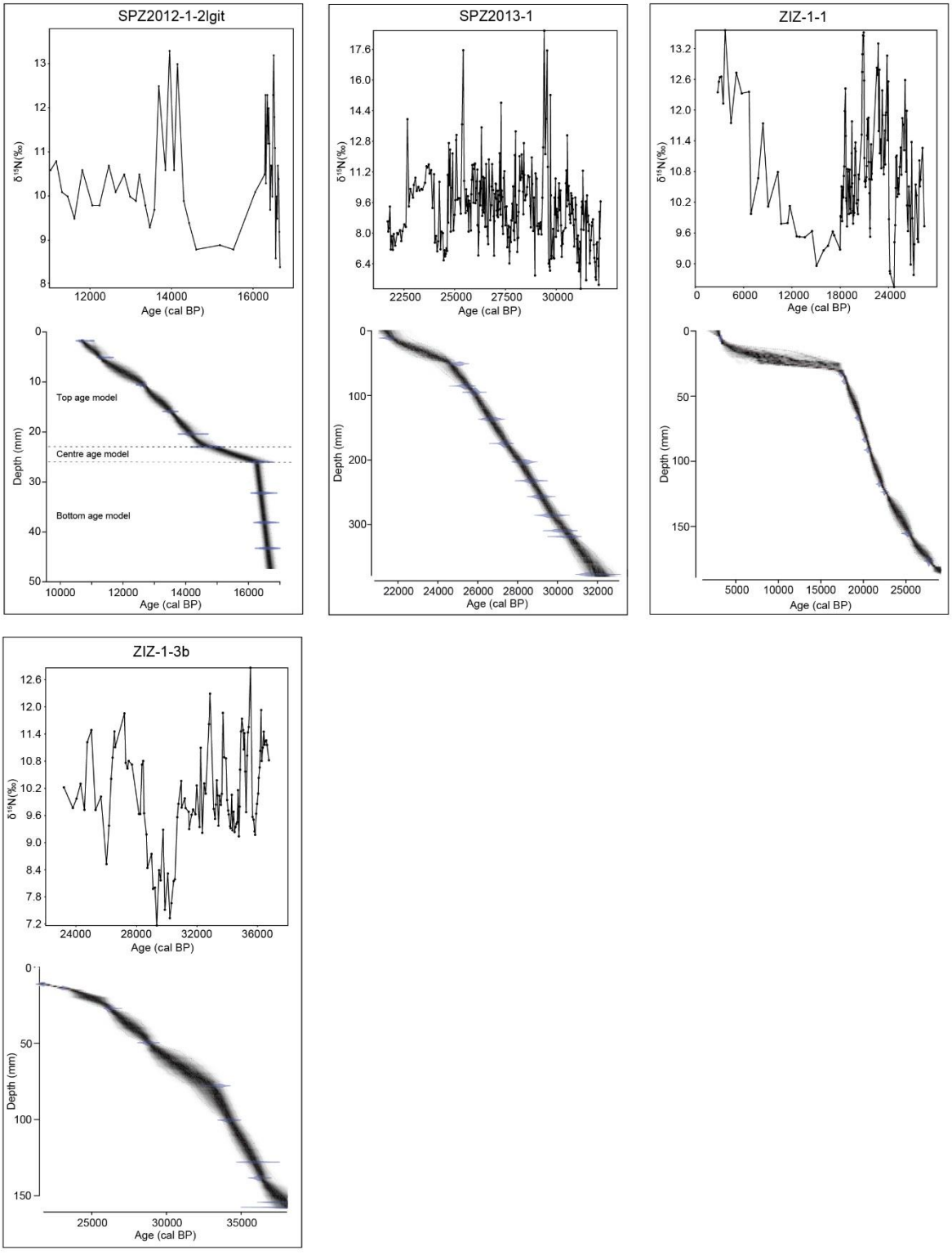

Figure. S1: $\delta^{15}N$ data and age models for each of the middens included in this study.

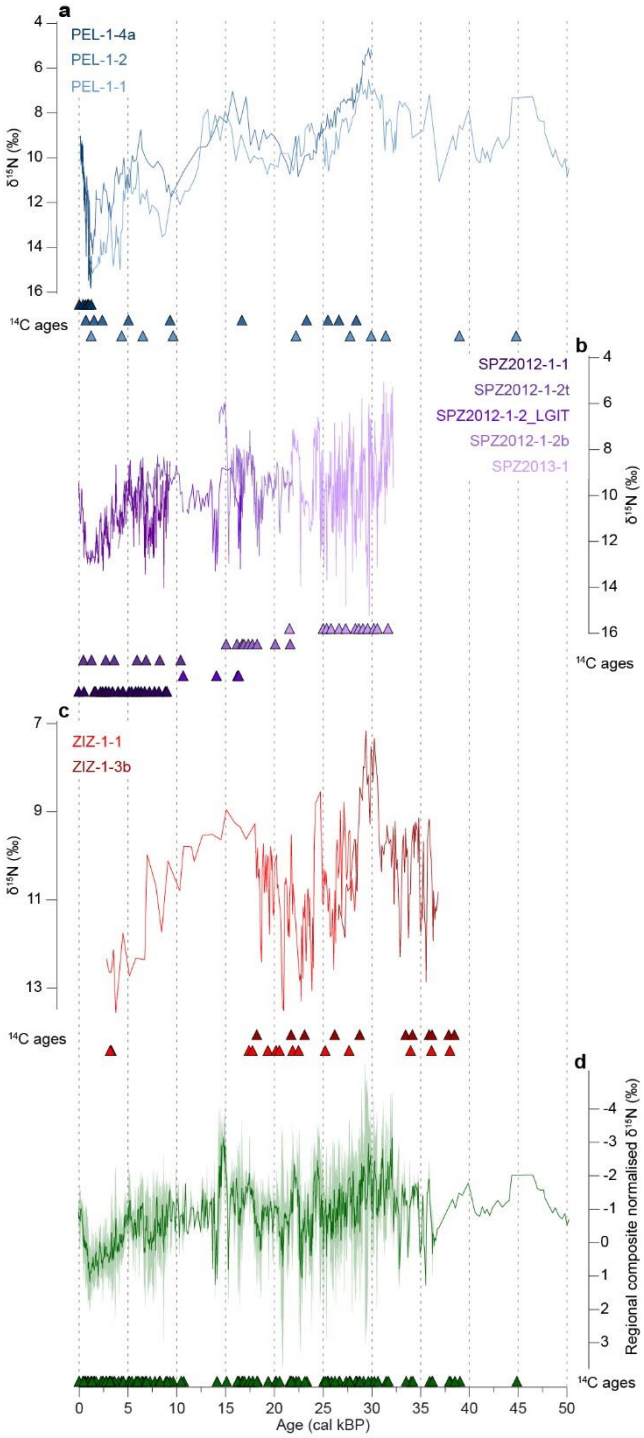

Figure S2: $\delta^{15}N$ records and radiocarbon ages (triangles, colours correspond to middens) from each hyrax midden from each of the sites considered, and the composite record established using Gaussian kernel smoothing (Rehfeld et al., 2011). As individual middens under the same climate regime exhibit differences in their isotopic records due to microclimatic influences (Carr et al., 2016) on individual foraging ranges (i.e. baseline $\delta^{15}N$ variability (Carr et al., 2016)), the $\delta^{15}N$ were normalised using standard scores to account for these differences prior to calculation of the composite record.

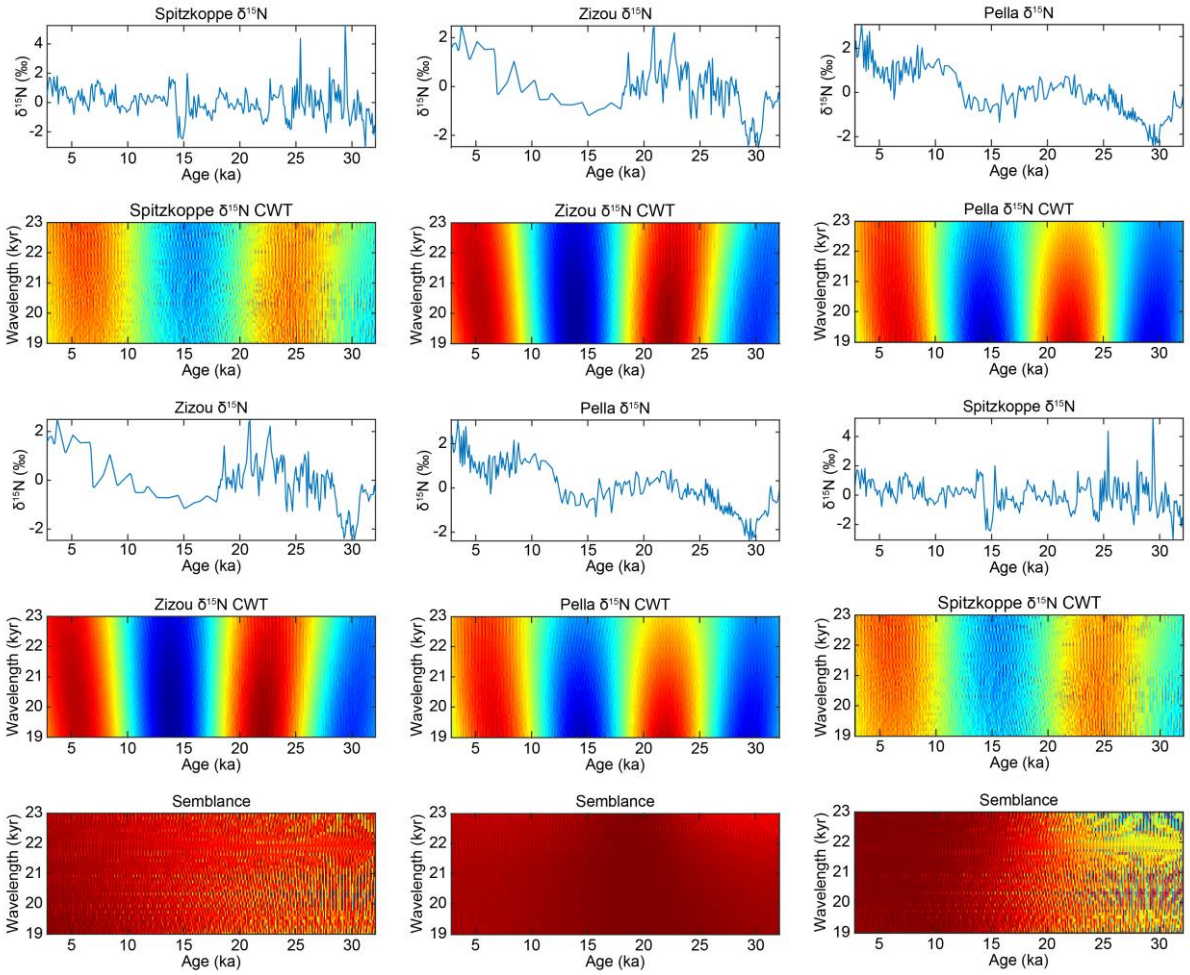

Figure. S3: Results of wavelet-based semblance analysis (Cooper and Cowan, 2008) of the $\delta^{15}N$ records from the three rock hyrax midden sites considered in this paper (interpolated to a common 100 year resolution, detrended using 2nd-order polynomial to remove the long-term glacial-interglacial pattern of ^{15}N enrichment, and clipped to a common length of 2800 – 32,100 cal BP). The heatmaps show the continuous wavelet transform results for the 19-23 kyr wavelengths related to orbital precession, which is the focus of this paper. In the upper two heatmaps, red indicates large positive anomalies while blue indicates large negative anomalies. In the lower semblance heatmaps, red indicates a semblance of +1 (positive correlation), and blue indicates a semblance of -1 (negative correlation). While high frequency, high amplitude variability dominates some parts of the individual records – particularly at Spitzkoppe - these analyses indicate coherent responses between the records at orbital frequencies.

References

Amundson, R., Austin, A. T., Schuur, E. A. G., Yoo, K., Matzek, V., Kendall, C., Uebersax, A., Brenner, D., and Baisden, W. T., 2003, Global patterns of the isotopic composition of soil and plant nitrogen: Global Biogeochemical Cycles, v. 17, no. 1.

Austin, A. T., and Vitousek, P. M., 1998, Nutrient dynamics on a precipitation gradient in Hawai'i: Oecologia, v. 113, no. 4, p. 519-529.

Blaauw, M., and Christen, J. A., 2011, Flexible paleoclimate age-depth models using an autoregressive gamma process: Bayesian Analysis, v. 6, no. 3, p. 457-474.

Bowen, G. J., 2008, Spatial analysis of the intra-annual variation of precipitation isotope ratios and its climatological corollaries: Journal of Geophysical Research: Atmospheres, v. 113, no. D5.

Carr, A. S., Chase, B. M., Boom, A., and Medina-Sanchez, J., 2016, Stable isotope analyses of rock hyrax faecal pellets, hyraceum and associated vegetation in southern Africa: Implications for dietary ecology and palaeoenvironmental reconstructions: Journal of Arid Environments, v. 134, p. 33-48.

Chase, B. M., Boom, A., Carr, A. S., Carré, M., Chevalier, M., Meadows, M. E., Pedro, J. B., Stager, J. C., and Reimer, P. J., 2015a, Evolving southwest African response to abrupt deglacial North Atlantic climate change events: Quaternary Science Reviews, v. 121, no. 0, p. 132-136.

Chase, B. M., Lim, S., Chevalier, M., Boom, A., Carr, A. S., Meadows, M. E., and Reimer, P. J., 2015b, Influence of tropical easterlies in southern Africa's winter rainfall zone during the Holocene: Quaternary Science Reviews, v. 107, no. 0, p. 138-148.

Chase, B. M., Meadows, M. E., Scott, L., Thomas, D. S. G., Marais, E., Sealy, J., and Reimer, P. J., 2009, A record of rapid Holocene climate change preserved in hyrax middens from southwestern Africa: Geology, v. 37, no. 8, p. 703-706.

Chase, B. M., Scott, L., Meadows, M. E., Gil-Romera, G., Boom, A., Carr, A. S., Reimer, P. J., Truc, L., Valsecchi, V., and Quick, L. J., 2012, Rock hyrax middens: a palaeoenvironmental archive for southern African drylands: Quaternary Science Reviews, v. 56, no. 0, p. 107-125.

Collins, J. A., Schefuß, E., Govin, A., Mulitza, S., and Tiedemann, R., 2014, Insolation and glacial–interglacial control on southwestern African hydroclimate over the past 140 000 years: Earth and Planetary Science Letters, v. 398, no. 0, p. 1-10.

Collins, W. D., Bitz, C. M., Blackmon, M. L., Bonan, G. B., Bretherton, C. S., Carton, J. A., Chang, P., Doney, S. C., Hack, J. J., Henderson, T. B., Kiehl, J. T., Large, W. G., McKenna, D. S., Santer, B. D., and Smith, R. D., 2006, The Community Climate System Model Version 3 (CCSM3): Journal of Climate, v. 19, no. 11, p. 2122-2143.

Cooper, G. R. J., and Cowan, D. R., 2008, Comparing time series using wavelet-based semblance analysis: Computers & Geosciences, v. 34, no. 2, p. 95-102.

Dansgaard, W., 1964, Stable isotopes in precipitation.: Tellus, v. 16, p. 436-447.

Farmer, E. C., deMenocal, P. B., and Marchitto, T. M., 2005, Holocene and deglacial ocean temperature variability in the Benguela upwelling region: implications for low-latitude atmospheric circulation.: Paleoceanography, v. 20, no. PA2018, p. doi:10.1029/2004PA001049.

Fordham, D. A., Saltré, F., Haythorne, S., Wigley, T. M. L., Otto-Bliesner, B. L., Chan, K. C., and Brook, B. W., 2017, PaleoView: a tool for generating continuous climate projections spanning the last 21 000 years at regional and global scales: Ecography, v. 40, no. 11, p. 1348-1358.

Garcin, Y., Schwab, V. F., Gleixner, G., Kahmen, A., Todou, G., Séné, O., Onana, J.-M., Achoundong, G., and Sachse, D., 2012, Hydrogen isotope ratios of lacustrine

sedimentary n-alkanes as proxies of tropical African hydrology: Insights from a calibration transect across Cameroon: Geochimica et Cosmochimica Acta, v. 79, p. 106-126.

Handley, L. L., Austin, A. T., Stewart, G. R., Robinson, D., Scrimgeour, C. M., Raven, J. A., Heaton, T. H. E., and Schmidt, S., 1999, The ^{15}N natural abundance ($\delta^{15}N$) of ecosystem samples reflects measures of water availability: Functional Plant Biology, v. 26, no. 2, p. 185-199.

He, F., Shakun, J. D., Clark, P. U., Carlson, A. E., Liu, Z., Otto-Bliesner, B. L., and Kutzbach, J. E., 2013, Northern Hemisphere forcing of Southern Hemisphere climate during the last deglaciation: Nature, v. 494, no. 7435, p. 81-85.

Herrmann, N., Boom, A., Carr, A. S., Chase, B. M., West, A. G., Zabel, M., and Schefuß, E., 2017, Hydrogen isotope fractionation of leaf wax n-alkanes in southern African soils: Organic Geochemistry, v. 109, p. 1-13.

Hogg, A. G., Hua, Q., Blackwell, P. G., Niu, M., Buck, C. E., Guilderson, T. P., Heaton, T. J., Palmer, J. G., Reimer, P. J., Reimer, R. W., Turney, C. S. M., and Zimmerman, S. R. H., 2013, SHCal13 Southern Hemisphere Calibration, 0–50,000 Years cal BP: Radiocarbon, v. 55, no. 4, p. 1889-1903.

Hou, J., D'Andrea, W. J., and Huang, Y., 2008, Can sedimentary leaf waxes record D/H ratios of continental precipitation? Field, model, and experimental assessments: Geochimica et Cosmochimica Acta, v. 72, no. 14, p. 3503-3517.

Little, M. G., Schneider, R. R., Kroon, D., Price, B., Bickert, T., and Wefer, G., 1997, Rapid palaeoceanographic changes in the Benguela Upwelling System for the last 160,000 years as indicated by abundances of planktonic foraminifera: Palaeogeography, Palaeoclimatology, Palaeoecology, v. 130, no. 1-4, p. 135-161.

Liu, Z., Otto-Bliesner, B. L., He, F., Brady, E. C., Tomas, R., Clark, P. U., Carlson, A. E., Lynch-Stieglitz, J., Curry, W., Brook, E., Erickson, D., Jacob, R., Kutzbach, J., and Cheng, J., 2009, Transient simulation of last deglaciation with a new mechanism for Bølling-Allerød warming: Science, v. 325, no. 5938, p. 310-314.

McCalley, C. K., and Sparks, J. P., 2009, Abiotic Gas Formation Drives Nitrogen Loss from a Desert Ecosystem: Science, v. 326, no. 5954, p. 837-840.

Murphy, B. P., and Bowman, D. M. J. S., 2006, Kangaroo metabolism does not cause the relationship between bone collagen $\delta^{15}N$ and water availability: Functional Ecology, v. 20, no. 6, p. 1062-1069.

Niedermeyer, E. M., Forrest, M., Beckmann, B., Sessions, A. L., Mulch, A., and Schefuß, E., 2016, The stable hydrogen isotopic composition of sedimentary plant waxes as quantitative proxy for rainfall in the West African Sahel: Geochimica et Cosmochimica Acta, v. 184, p. 55-70.

Otto-Bliesner, B. L., Russell, J. M., Clark, P. U., Liu, Z., Overpeck, J. T., Konecky, B., deMenocal, P., Nicholson, S. E., He, F., and Lu, Z., 2014, Coherent changes of southeastern equatorial and northern African rainfall during the last deglaciation: Science, v. 346, no. 6214, p. 1223-1227.

Pichevin, L., Cremer, M., Giraudeau, J., and Bertrand, P., 2005, A 190 kyr record of lithogenic grain-size on the Namibian slope: forging a tight link between past wind-strength and coastal upwelling dynamics: Marine Geology, v. 218, no. 1-4, p. 81-96.

Rehfeld, K., Marwan, N., Heitzig, J., and Kurths, J., 2011, Comparison of correlation analysis techniques for irregularly sampled time series: Nonlin. Processes Geophys., v. 18, no. 3, p. 389-404.

Sachse, D., Billault, I., Bowen, G. J., Chikaraishi, Y., Dawson, T. E., Feakins, S. J., Freeman, K. H., Magill, C. R., McInerney, F. A., van der Meer, M. T. J., Polissar, P., Robins, R., Sachs, J. P., Schmidt, H.-L., Sessions, A. L., White, J. W. C., West, J. B., and

Kahmen, A., 2012, Molecular paleohydrology: interpreting the hydrogen-isotopic composition of lipid biomarkers from photosynthetic organisms: Annual Review of Earth and Planetary Sciences, v. 40, no. 1, p. null.

Schefuß, E., Schouten, S., and Schneider, R. R., 2005, Climatic controls on central African hydrology during the past 20,000 years: Nature, v. 437, no. 7061, p. 1003-1006.

Sessions, A. L., Burgoyne, T. W., and Hayes, J. M., 2001, Determination of the H_3 factor in hydrogen isotope ratio monitoring mass spectrometry: Analytical Chemistry, v. 73, no. 2, p. 200-207.

Shackleton, N. J., 2000, The 100,000-Year Ice-Age Cycle Identified and Found to Lag Temperature, Carbon Dioxide, and Orbital Eccentricity: Science, v. 289, no. 5486, p. 1897-1902.

Slota, P. J., Jull, A. J. T., Linick, T. W., and Toolin, L. J., 1987, Preparation of small samples for ^{14}C accelerator targets by catalytic reduction of CO: Radiocarbon, v. 29, p. 303-306.

Stuut, J.-B. W., Prins, M. A., Schneider, R. R., Weltje, G. J., Jansen, J. H. F., and Postma, G., 2002, A 300 kyr record of aridity and wind strength in southwestern Africa: inferences from grain-size distributions of sediments on Walvis Ridge, SE Atlantic: Marine Geology, v. 180, no. 1-4, p. 221-233.